

Growth of large area graphene from sputtered films

Genhua Pan¹, Mark Heath¹, David Horsell² and M. Lesley Wears²*

¹ Wolfson Nanomaterials & Devices Laboratory, Faculty of Science and Technology, University of Plymouth, Devon, PL4 8AA, UK

² College of Engineering, Mathematics and Physical Sciences, University of Exeter, Exeter, EX4 4QF, UK

Techniques for mass-production of large area graphene using an industrial scale thin film deposition tool could be the key to the practical realization of the wide range of technological applications of the material¹⁻⁵. Since the discovery of graphene⁶, considerable progress in new production methods of graphene has been made, which includes chemical vapour deposition of graphene on metal substrates⁷⁻¹³ and epitaxial growth of graphene by thermal decomposition of single crystal SiC substrate under ultrahigh vacuum and very high temperature¹⁴. However, growth of graphene from sputtered carbon sources has not been reported. Here we demonstrate the growth of large area polycrystalline graphene from a sputtered carbon-containing layer (SiC or C) either underneath or atop a metal layer (Ni or Pt) by in-situ or ex-situ rapid thermal processing at temperatures ranging from 650 °C to 1000 °C. We also demonstrate in principle a potential route to mass-production of graphene on insulator, which could pave the way to an easy integration of graphene into modern semiconductor device process flows.

Graphene, a two-dimensional material composed of a single layer of carbon atoms, has attracted huge amount of interests due to its wide range of novel applications^{1,6}. The successful development of these devices depends largely on the large scale production of high quality graphene on device compatible substrates using thin film deposition techniques commonly used in semiconductor device processes. To date, large-area growth of polycrystalline graphene by CVD has been achieved on metal substrates such as ruthenium⁷, iridium⁸, platinum⁹, nickel^{10,12} and copper¹¹, or even in the absence of a substrate¹⁵. Though suitable for mass production¹⁶, the need for transferring the films to different substrates¹³ constrains its use in many applications¹⁷. Although epitaxial graphene¹⁴ has been demonstrated a viable route for the development of electronic devices, such as field effect transistors¹⁸, it has a number of unsatisfactory features including the lack of continuity and uniformity of the graphene film¹⁹ and small domain sizes (30~200nm)²⁰. Also, the graphene is grown on the single crystal SiC substrate only, which is expensive and also semi-insulating. Graphene has also been synthesised via the SiC route by using rapid thermal processing (RTP) at a temperature of 1100 °C²¹. Lower temperature synthesis of few- layers graphene has also been reported by deposition of a Ni layer atop single crystal SiC substrate with RTP temperatures around 750 °C²².

To date, graphene has yet to be produced from sputtered carbon sources despite sputtering being one of the most common and versatile thin film production tools. Here we show the growth of large area graphene from sputtered SiC or C films either atop or underneath a metal layer (Ni or Pt). We also demonstrate the feasibility of transferring the graphene to a different insulator substrate by subsequent vacuum deposition, which could potentially lead to the production of graphene on insulator (GoI) wafers.

Fig.1 is a schematic illustration of our graphene growth process. A carbon containing film (SiC or C) and a metal film (Ni, or Pt) were deposited by sputtering on to a Si substrate in the order of either substrate/carbon/metal, Fig.1a, or substrate/metal/carbon, Fig.1b (here we concentrate on SiC and Ni only). After deposition, the stacks were subject to an RTP which was carried out either inside the same deposition chamber (in-situ), or in a separate RTP machine (ex-situ), see Methods and section 1 of Supplementary Information for detail. We found that graphene always grows on the top surface of the stack, irrelevant of the deposition sequence of the two layers, Fig.1c. After RTP, two possible routes for transferring the graphene to insulating substrates were used, as shown in Fig.1 d and e, or Fig.1f, respectively. In Fig.1f, the Ni-silicide is dissolved in an HCl solution and the graphene settles on the Si substrate as loosely adhered film, which is an approach already employed^{12,21,22}. In Fig.1d & e, we show a new approach to the potential production of GoI wafers by combining this graphene growth method with the standard Si wafer fabrication techniques²³. An SiO₂ layer serving as a new substrate for the graphene is deposited on to the as-grown graphene in the same evacuation by sputtering after the RTP and a supporting substrate (usually Si wafer) can then be directly bonded to the new insulator, Fig.d. The GoI is obtained, as shown in Fig.1e, after the removal of the original substrate by a Si etcher and the Ni-silicide, in an acid solution.

Fig.2a is a typical Raman spectrum of the as-grown graphene (red) from a sample of substrate/SiC(50nm)/Ni(500nm) with ex-situ RTP at 1000 °C for 2 minutes (we refer to it as S1). A spectrum of mechanically exfoliated monolayer graphene (MEG) obtained by the same spectrometer is also shown (in blue) for comparison. There are two main peaks present on both spectra: the G and 2D bands. Their peak positions, G/2D intensity ratio and full width at half maximum (FWHM) are given in the figure for direct comparison. It is well known that the value of FWHM of the symmetric 2D band or the intensity ratio of the G and

2D peak can be used to determine the number of layers^{17,24,25}, with typical values of FWHM $<35\text{ cm}^{-1}$ and G/2D <0.5 for monolayer graphene. As can be seen, both the FWHM and the G/2D ratio of the spectrum of the graphene grown from sputtered films indicate a monolayer. These values are smaller than that of epitaxial graphene²⁵ and, surprisingly, even smaller than that of MEG shown in the figure. Fig.2b shows a mapping of the FWHM for an area of 1x0.7 mm of S1. The estimated monolayer surface coverage of the sample is around 40% for the mapped area. The lack of D band at 1350 cm⁻¹ and the almost identical G peak position of the two spectra indicate that the monolayer graphene has few defects or large grains²⁴. An optical microscope image of the as-grown sample is shown in Fig.2c, where the monolayer graphene is visible as the light-brown coloured areas. Detailed surface morphology can be seen from the AFM image of Fig.2d. The typical grain size of the film is around 2 μm . The areas of graphene of the samples are visually identifiable, as shown by the camera shots in Fig.2e and f for two samples with the same layer thicknesses but different layer deposition sequence. The shiny or dark areas are covered by graphene whilst the dull or grey areas are covered by amorphous carbon. As can be seen, samples with SiC atop Ni, Fig.2f, produced much better graphene surface coverage than the samples with SiC underneath the Ni, Fig.2e, reaching nearly 99% for the sample size shown in Fig.2f. X-ray diffraction examination of the shiny and dull regions showed no significant difference in terms of phase structure and crystal texture (see Fig.S2 for detail).

Graphene was grown from samples with various layer thicknesses, deposition sequences and RTP conditions with typical results shown in Figure 3. Fig.3a shows two Raman spectra of sample S2 (sub/SiC(50nm)/Ni(200nm)) processed with in-situ RTP (red) and ex-situ RTP (blue), respectively. (for key differences and typical heating cooling curves of the two different RTP systems, please refer to section 1 of Supplementary Information and Fig.S1). As can be seen, although graphene were produced in both RTP systems, in particular by

the in-situ RTP with temperature as low as 650 °C, the spectrum for the graphene by in-situ RTP has a FWHM value of the 2D band of 74.1 cm⁻¹ and G/2D intensity ratio of 1.77, both indicating several-layer graphene²⁴. The D/G intensity ratio of 0.17 also suggests that the graphene contains considerable nano-grains²⁶. The AFM images for the sample, Fig3a.1 and (a.2), confirms that the re-crystallisation process of the sample was incomplete with a large portion of the areas containing nano-grains with typical sizes of 20~30nm, Fig.3a.2. On the other hand, the same sample processed by ex-situ RTP (peak intensity of 68% for 2 minutes, which gave maximum temperature of 1000 °C, see Fig.S1 for its heating & cooling curve) produced graphene with much better Raman spectrum (FWHM value of 47 cm⁻¹ and G/2D intensity ratio of 0.96), indicating bi-layer graphene. The AFM image of Fig.3a.3 shows that the sample is well crystallised with typical grain sizes in the range of 1 - 2.5nm.

Fig.3b shows the Raman spectra for two samples (S3 and S4), with the same SiC and Ni layer thicknesses but different deposition sequence and ex-situ RTP conditions. S3 has SiC underneath Ni and S4 has a reversed layer sequence with SiC atop Ni. The top two spectra are for S3 and S4 with RTP peak power intensity of 68% for 2 minutes, as for the ex-situ RTP for S2 in Fig.3a. As can be seen, a spectrum of good quality monolayer graphene was obtained for S3. The spectrum of S4 shows increased FWHM and G/2D ratio. However, the graphene surface coverage of graphene for S3 and S4 are different with S4 showing much better coverage than S3, as already shown by the photo shots in Fig.2f and e, respectively. It is also worth noting that the spectrum of S3 is also much better than that for S2 prepared in the same ex-situ RTP conditions (spectrum in blue in Fig.3a), suggesting that thicker Ni films (500nm) favours the growth of higher quality monolayer graphene in the same RTP conditions. The two spectra at the bottom of Fig.3b are for S3 and S4 processed with ex-situ RTP at a lower annealing temperature of 700 °C (with RTP peak power intensity of 10% for 2 minutes). As can be seen, the FWHM values of the two spectra are 45.8 cm⁻¹ and 55.2 cm⁻¹,

respectively, suggesting bi- or tri-layer graphene. Again, S3 (Ni atop SiC) exhibits slightly better Raman characteristics with smaller FWHM values and nearly negligible D band intensity.

Fig.3c shows two Raman spectra of S4 prepared under the same 68% power intensity for 2 minutes but with slower cooling rate at 2%/s and 1%/s for the top and bottom spectrum, respectively. As is shown, these samples exhibit much wider 2D band and also higher D band intensity in comparison with the green spectrum of Fig.3b, which has the same layer structure and annealing temperature and time, but faster cooling rate. It was found that a heating rate is not crucial to the growth of graphene, but a faster cooling rate favours the growth of fewer layer graphene, which agrees with the results by Yu et al¹².

The crystal structure and crystallographic orientation of the films were examined by small angle grazing-incidence diffraction (GID) of x-rays, please refer to section 2 of Supplementary Information and Fig.S2 for more information about GID. Figure 4 shows the GID patterns of three selected samples corresponding to S3, S4 and S2 above together with their corresponding Raman spectrum for reference. As already stated, S3 and S4 have the same layer thicknesses of SiC and Ni but reversed layer sequence and both were prepared by ex-situ RTP at 1000 °C for 2 minutes, as those for upper two spectra in Fig.3b. As can be seen, all three samples exhibit preferred Ni(111) and Ni₁₇Si₃(220) orientations, indicating good crystallites and complete Ni-silicidation. The contrast difference in peak intensities of the Ni(111), Ni(200) and Ni₁₇Si₃(220) of the two samples, as shown by panels (a) and (b), suggests that there is a composition distribution gradient of the Ni-silicide across the depth of the films, being the top surface of S3 Ni rich, and that of S4 Ni-silicide rich, because the structures on the top surface contributes more to the intensities of the diffraction peaks in GID. This is natural considering the different layer deposition sequence of the two samples

and the relatively short RTP time (2 minutes), which was insufficient for a complete diffusion of the SiC throughout the whole 500nm depth of the Ni film. It is also natural to believe that the carbon concentration across the film depth is also non-uniform. This is further confirmed by more x-ray diffraction analysis as shown in Fig.S2 and section 2 of Supplementary Information. This may explain that the better surface coverage of graphene of S4, refer to Fig.2f and e, is due to its top surface is much carbon richer than that in S3. The richer carbon concentration on the top surface of S4 may also contribute to the formation of more monolayers of graphene in the graphene growth temperature and time window during cooling down. On the other hand, there is insufficient carbon concentration on the top surface of S3, which favours the growth of monolayer graphene but results in lower surface coverage. We therefore believe a delicate balance can be achieved by optimising the thickness ratio of the two films, by which monolayer graphene with a desirable surface coverage can be realised across the whole wafer surface. The existence of the $\text{Ni}_{17}\text{Si}_3(220)$ phase doesn't appear to have any adverse effect on the growth of graphene. Panel (c) is the GID pattern for S2, which has the same SiC thickness of 50nm but with thinner Ni layer of 200nm and prepared with in-situ RTP at 650 °C, as those for Fig.3a. The major difference in the GID pattern of S2 is the presence of an additional peak of Si(311) and a relatively weaker and messy Ni(200) band. This may suggests that the recrystallization and Ni silicidation processes of the sample were incomplete due to the relatively lower RTP temperature. This interpretation agrees with the AFM images of Fig.3a, where nano-crystalline grains exists in large portion of the sample.

As mentioned above (Fig.1), amorphous carbon material can also be used in place of SiC as a carbon source and carbon absorbing noble metals, such as Pt can be used in place of Ni for the growth of graphene. Some initial results on these are shown in Fig.S3 of Supplementary Information. Work on this is on-going. The different combination of materials may provide

more options for the optimisation of the growth process for large scale and high quality monolayer graphene at a much reduced cost.

As already shown in Fig.1d and e, and Fig.1f, respectively, two approaches can be used for the transfer of graphene onto different insulating substrates. Fig.5a is a typical Raman spectrum of the transferred graphene, after the removal of the Ni and Ni-silicide layers in HCl and settled on a piece of Si wafer. In comparison with the Raman spectrum of the as-grown graphene of the same sample (refer to the green spectrum of Fig.3b), there is almost no change in the relative intensities of G and 2D peak and the value of FWHM of the 2D band, however, the D peak intensity of the transferred graphene is slightly higher, which may be due to damages caused by the handling of the graphene film in the transfer process. A typical optical microscope image of the transferred graphene on Si wafer is shown in Fig.5a.1. We have found that on the microscopic scale, the transferred graphene is not smooth but a 3D replica or a rigid footprint of the Ni surface morphology on which it grew. Due to the strength of the π -bond, such a replica is a quite rigid structure. Fig.5a.2 is an AFM image of the surface morphology of the transferred graphene from S4, which shows well defined grains with typical sizes in the range of 1-2 μm . It appears that it is impossible to grow graphene directly onto an insulator substrate via this route because the graphene is grown with atomic contact with the Ni or Ni-silicide surface. We have attempted the direct growth of graphene by covering the SiC/Ni or Ni/SiC samples with a Si wafer during RTP, but no graphene was obtained on the Si wafer covers.

To demonstrate in principle the feasibility of producing graph GoI by sputtering, as already shown in Fig.1d and e, new insulating layers of SiO₂(200nm)/Ti(200nm)/SiO₂(200nm) were deposited onto the graphene after RTP (for reasons why this stack was chosen, please refer to section 4 of Supplementary Information for detail). The deposition of the SiO₂ was carried

out using a magnetron target with the initial layers of the SiO_2 sputtered with power as low as 50 W to minimise the potential damage of plasma and high energy sputtering particles to the graphene, if any as reported by others²⁷⁻²⁹. A piece of heat release tape is then applied to the top of the wafer as an additional supporting substrate to the GoI (to replace the direct wafer bonding as described in Fig.1, in the lack of such a specialist wafer-fab facility). The stack can then be pulled off from the original substrate due to the relatively poor adhesion of Ni to the original substrate (ideally, the original substrate needs to be removed by a Si etcher, which is a standard process in a wafer-fab). Fig.4b is a typical Rama spectrum (in red) of the GoI supported on a piece of heat-release tape after the removal of Ni and Ni-silicide layers in HCl solution. For comparison, a Raman spectrum of the as-grown graphene from the same sample is also shown (in blue). As can be seen, the FWHM value of the GoI on tape has increased to 51.8 cm^{-1} in comparison with 46.6 cm^{-1} of the as-grown graphene. There is also a considerable increase of the D peak intensity, which indicates possible damages of the GoI, which may be caused by a number of factors, including the distortions of the tape by the pulling off force and by the laser heating effect to the supporting tape during Raman, and the potential damage caused by the sputter-deposition of the new insulator. A digital camera photo shot of a whole piece of the peeled-off sample on tape is shown in b.1. Some wrinkles and damages were evident, which were due to the strain applied to the tape by pulling off. An optical microscope image of the GoI surface after etching of the Ni-silicide in HCl is shown in b.2.

In conclusion, we have shown that large area polycrystalline graphene can be grown from sputtered Ni film with SiC either underneath or on top of the Ni layer with in-situ or ex-situ RTP at temperatures ranging from $650 \text{ }^\circ\text{C}$ to $1000 \text{ }^\circ\text{C}$. It was found that graphene always grew on the top surface of the stack and in close atomic contact with the Ni or Ni-silicide. Excellent Raman spectra for monolayer graphene were obtained for samples under optimised

conditions. A fast cooling rate is essential to the formation of monolayer graphene. Raman mapping has shown a 40% monolayer surface coverage for an area of 1x0.7mm². The areas with graphene grown on the sample are visibly obvious. Samples with Ni atop SiC produced the best monolayer graphene spectra whilst samples with Ni underneath the SiC produced the best surface coverage of graphene for up to 99% across a sample area of 20x12 mm². The difference in the graphene growth from the films of the two different layer deposition sequences and the flexibility of the sputtering process in making films of different thickness combinations may provide the possibility of process optimisation for the growth of large scale and good surface coverage of monolayer graphene. We have also in principle demonstrated the feasibility of transferring graphene to a different insulator substrate by vacuum deposition of insulator materials directly on to the graphene after RTP for a potential route to the production of GoI. However, due to the limitations of the available facilities for the work, such a feasibility demonstration is far from perfect. Further work is required to optimise such a process in a number of areas for the eventual realisation of GoI wafer for device applications.

Methods

The deposition of films was carried out in an RF diode and magnetron sputtering machine with three sputtering targets. The typical base pressure was 2×10^{-7} Torr and Ar pressure for deposition, 3 mTorr. The deposition rate at 300 W was 12.5 nm/m for SiC, 6.1 nm/m for Ni, 6nm/m for C, 7.3nm/m for Pt and 17.5 nm/m for SiO₂, respectively, as calibrated by AFM. All targets have a typical purity of 99.95%. No substrate heating was applied during the deposition of all the layers. The substrates used in the work were single side polished Si wafers with a 300nm-thick thermally oxidised SiO₂ layer, which was referred to as substrate or Si wafer throughout the paper.

Samples were rapid thermal processed either in-situ or ex-situ. The in-situ RTP was carried out in the same vacuum chamber as the sputter-deposition using a 500W halogen lamp and the sample was heated for 10 minutes to reach a maximum temperature of 650 °C before cooling down naturally by switching off the halogen lamp, see Fig.S1 for heating and cooling curves. The in-situ RTP used in the work has a considerably slower heating and cooling rate. Due to the limited heating power available and the huge thermal-mass of the substrate holder, there isn't too much flexibility to alter the heating and cooling rate in the existing machine to achieve the optimum RTP conditions required for the monolayer graphene growth. The best graphene films were grown using ex-situ RTP.

The ex-situ RTP was carried out in a commercial RTP apparatus with a quartz chamber. The RTP apparatus provides a much faster heating and cooling rate (see Fig.S1 for typical heating and cooling curves). This is because there are eleven 1.5 kW halogen lamps available for rapid temperature ramp up at a typical rate of 100 °C/s for up to 1200 °C. It also has a rapid cooling capability due to a cold chamber wall design and a very small thermal mass of the quartz sample holder. It can operate in either intensity or temperature mode. In the intensity mode, users can specify the ramp-up and ramp-down rate, maximum intensity as percentage of total power per second, and annealing time. In the temperature mode, the user can define annealing time and temperature but without the control for ramp-up and

ramp-down rate. The intensity mode is mainly used in this work. The sample chamber was purged with Ar gas for one hour before the RTP process. We found this is necessary to prevent the potential oxidation of the sample. In order to achieve the growth of good quality graphene, samples need to be annealed fresh, particularly for samples with Ni on top. In both RTP systems, the temperatures were measured by a thermal couple cemented on the film side surface of the wafers within the lamp heating range.

As-grown and transferred graphene films were examined by Raman spectroscopy (with a 532nm laser). Film thicknesses and surface morphology were characterised by AFM. Bragg-Brentano geometry and grazing-incidence x-ray diffraction at 1° angle of incidence were used for the microstructural and crystallographic characterisation of the metal and SiC films.

- 1 Geim, A. K. Graphene: Status and Prospects. *Science* **324**, 1530-1534, doi:DOI 10.1126/science.1158877 (2009).
- 2 Geim, A. K. & Novoselov, K. S. The rise of graphene. *Nat Mater* **6**, 183-191 (2007).
- 3 Liao, L. *et al.* High-speed graphene transistors with a self-aligned nanowire gate. *Nature* **467**, 305-308, doi:<http://www.nature.com/nature/journal/v467/n7313/abs/nature09405.html#supplementary-information> (2010).
- 4 Lin, Y.-M. *et al.* 100-GHz Transistors from Wafer-Scale Epitaxial Graphene. *Science* **327**, 662, doi:10.1126/science.1184289 (2010).
- 5 Castro Neto, A. H., Guinea, F., Peres, N. M. R., Novoselov, K. S. & Geim, A. K. The electronic properties of graphene. *Reviews of Modern Physics* **81**, 109-162 (2009).
- 6 Novoselov, K. S. *et al.* Electric field effect in atomically thin carbon films. *Science* **306**, 666-669, doi:DOI 10.1126/science.1102896 (2004).
- 7 Sutter, P. W., Flege, J. I. & Sutter, E. A. Epitaxial graphene on ruthenium. *Nature Materials* **7**, 406-411, doi:Doi 10.1038/Nmat2166 (2008).
- 8 Coraux, J., N'Diaye, A. T., Busse, C. & Michely, T. Structural coherency of graphene on Ir(111). *Nano Letters* **8**, 565-570, doi:Doi 10.1021/Nl0728874 (2008).
- 9 O. Ryoko & *et al.* Electronic States of Monolayer Graphene on Pt(755) and TiC(755). *Tanso* **195**, 400-404 (2000).
- 10 Kim, K. S. *et al.* Large-scale pattern growth of graphene films for stretchable transparent electrodes. *Nature* **457**, 706-710, doi:http://www.nature.com/nature/journal/v457/n7230/supplinfo/nature07719_S1.html (2009).
- 11 Li, X. S. *et al.* Large-Area Synthesis of High-Quality and Uniform Graphene Films on Copper Foils. *Science* **324**, 1312-1314, doi:DOI 10.1126/science.1171245 (2009).
- 12 Yu, Q. *et al.* Graphene segregated on Ni surfaces and transferred to insulators. *Applied Physics Letters* **93**, 113103-113103 (2008).
- 13 Ismach, A. *et al.* Direct Chemical Vapor Deposition of Graphene on Dielectric Surfaces. *Nano Letters* **10**, 1542-1548, doi:10.1021/nl9037714 (2010).

14 Berger, C. *et al.* Ultrathin epitaxial graphite: 2D electron gas properties and a route toward graphene-based nanoelectronics. *J Phys Chem B* **108**, 19912-19916, doi:Doi 10.1021/Jp040650f (2004).

15 Dato, A., Radmilovic, V., Lee, Z., Phillips, J. & Frenklach, M. Substrate-free gas-phase synthesis of graphene sheets. *Nano Letters* **8**, 2012-2016, doi:Doi 10.1021/Nl8011566 (2008).

16 Bae, S. *et al.* Roll-to-roll production of 30-inch graphene films for transparent electrodes. *Nat Nano* **5**, 574-578, doi:<http://www.nature.com/nnano/journal/v5/n8/abs/nnano.2010.132.html#supplementary-information> (2010).

17 Emtsev, K. V. *et al.* Towards wafer-size graphene layers by atmospheric pressure graphitization of silicon carbide. *Nat Mater* **8**, 203-207, doi:http://www.nature.com/nmat/journal/v8/n3/supplinfo/nmat2382_S1.html (2009).

18 Moon, J. S. *et al.* Epitaxial-Graphene RF Field-Effect Transistors on Si-Face 6H-SiC Substrates. *Electron Device Letters, IEEE* **30**, 650-652 (2009).

19 Hibino, H. *et al.* Microscopic thickness determination of thin graphite films formed on SiC from quantized oscillation in reflectivity of low-energy electrons. *Physical Review B* **77**, 075413 (2008).

20 Hass, J. *et al.* Highly ordered graphene for two dimensional electronics. *Applied Physics Letters* **89**, 143106-143103 (2006).

21 Hofrichter, J. *et al.* Synthesis of Graphene on Silicon Dioxide by a Solid Carbon Source. *Nano Letters* **10**, 36-42, doi:10.1021/nl902558x (2009).

22 Juang, Z.-Y. *et al.* Synthesis of graphene on silicon carbide substrates at low temperature. *Carbon* **47**, 2026-2031, doi:10.1016/j.carbon.2009.03.051 (2009).

23 Maleville, C. & Mazure, C. Smart-Cut (R) technology: from 300 mm ultrathin SOI production to advanced engineered substrates. *Solid-State Electronics* **48**, 1055-1063, doi:DOI 10.1016/j.sse.2003.12.029 (2004).

24 Ferrari, A. C. *et al.* Raman Spectrum of Graphene and Graphene Layers. *Physical Review Letters* **97**, 187401 (2006).

25 Lee, D. S. *et al.* Raman Spectra of Epitaxial Graphene on SiC and of Epitaxial Graphene Transferred to SiO₂. *Nano Letters* **8**, 4320-4325, doi:10.1021/nl802156w (2008).

26 Cancado, L. G. *et al.* General equation for the determination of the crystallite size L_[sub a] of nanographite by Raman spectroscopy. *Applied Physics Letters* **88**, 163106-163103 (2006).

27 Dimiev, A. *et al.* Layer-by-Layer Removal of Graphene for Device Patterning. *Science* **331**, 1168-1172, doi:10.1126/science.1199183 (2011).

28 Xue Peng Qiu, Y. J. S., Jing Niu, Narayananpillai Kulothungasagaran, Gopinadhan Kalon, Caiyu Qiu, Ting Yu, Hyunsoo Yang. Disorder-free sputtering method on graphene. <http://arxiv.org/abs/1208.1835v1> (2012).

29 Miriam, F. *et al.* Versatile sputtering technology for Al₂O₃ gate insulators on graphene. *Science and Technology of Advanced Materials* **13**, 025007 (2012).

Acknowledgment

The authors wish to acknowledge Mr Evgeny Alexeev for his assistance on Raman mapping.

Author contributions

Genhua Pan developed the project ideas, planning of the project and associated equipment, supervision of researcher, AFM imaging and some of the sputtering, RTP and Raman work, analysis of results and writing of the paper.

Mark Heath Carried out most of the experimental work on sputtering and Raman spectroscopy.

David Horsell contributed to analysis of Raman spectra, discussions and paper reviewing.

Lesley Wears carried out the x-ray diffraction experiment.

Figures

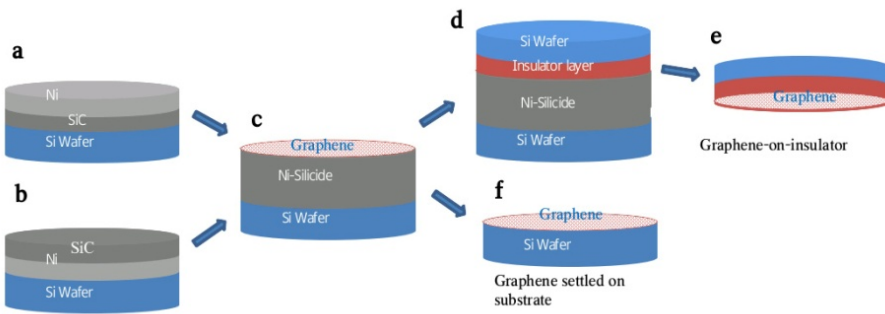


Figure 1| Schematic illustration of the graphene growth process. Sputter deposition of a carbon containing layer (SiC or C) and a metal film (Ni or Pt) on a Si wafer in the order of either SiC/Ni **a**, or Ni/SiC **b**. **c**, Rapid thermal processing resulting in Ni-silicidation and formation of graphene atop the Ni-silicides upon cooling. The graphene film can then be made as Gol by deposition of a new insulator material on graphene, direct bonding of Si wafer **d**. And removal of the original wafer and the Ni-silicide layer **e**. **f**, The graphene can also be settled on the original Si wafer after dissolving the Ni-Silicides from **c**.

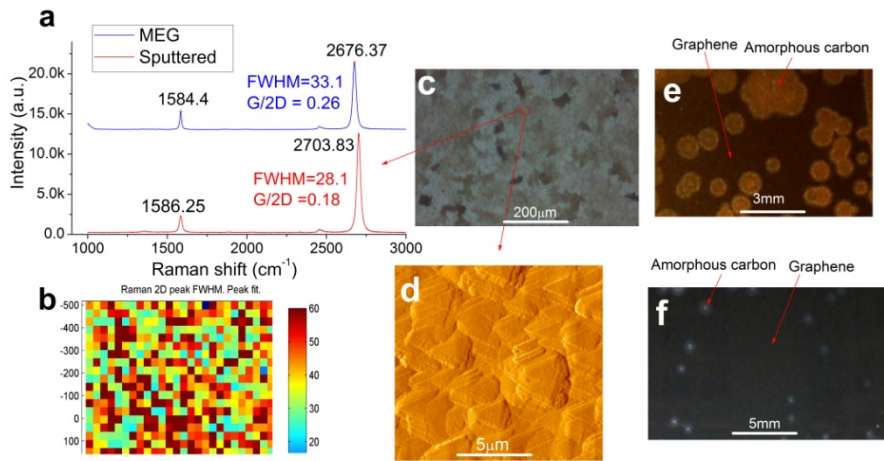


Figure 2| Typical characteristics of as-grown graphene. **a**, Raman spectrum of as-grown graphene (red) of S1(sub/SiC(50nm)/Ni500(nm)) showing the monolayer features, a reference spectrum of mechanically exfoliated monolayer graphene (MEG) on Si/SiO₂ substrate measured by the same Raman spectrometer is also shown for comparison (blue), both spectra were normalised with the same G peak height. **b**, Raman mapping of FWHM of 2D band for a sample area of 1x0.7mm showing 40% monolayer surface coverage. **c**, Optical microscope image of the sample surface, where graphene appears as light-brownish colour. **d**, AFM image of the polycrystalline graphene surface showing typical grain sizes of 1.5-2.5 μm. **e**, Digital camera shot of S1 surface showing visually distinctive areas with graphene and without graphene. **f**, Digital camera shot of a sample with layer structure of sub/Ni500(nm)/SiC(50nm), which is in reversed layer deposition sequence from S1, showing a much better surface coverage of graphene on the wafer.

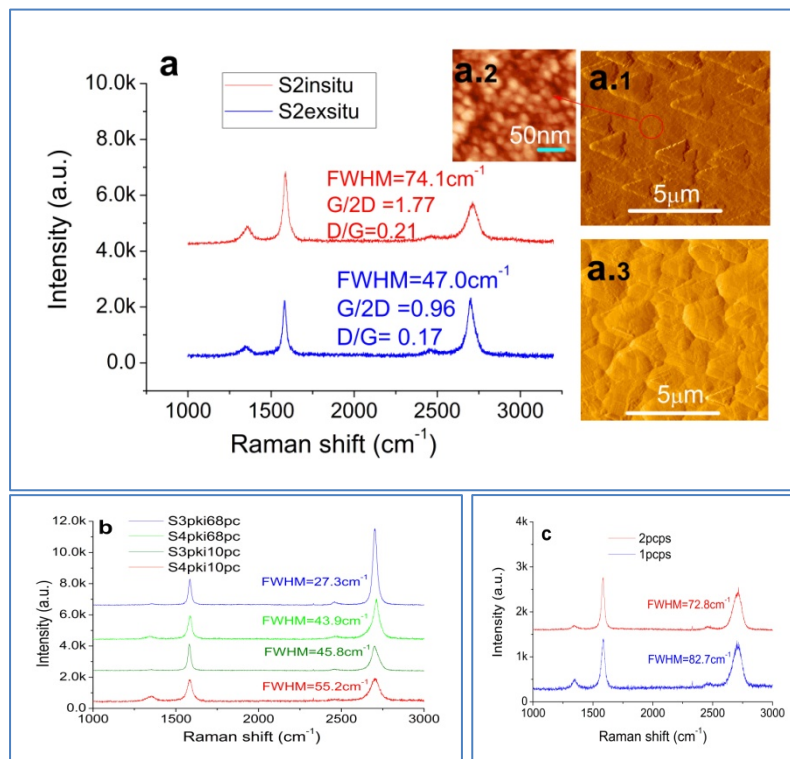


Figure 3| Raman spectra of as-grown graphene from samples with different Ni layer thicknesses, deposition sequences and RTP systems/conditions. **a**, Raman spectra of S2 (SiC50nm/Ni200nm) with in-situ (red) and ex-situ (blue) RTP. AFM images for S2 in-situ are given in **(a.1)** and **(a.2)**, and S2 ex-situ in **(a.3)**. **b**, Raman spectra of samples S3 and S4 (with the same SiC and Ni thicknesses but reversed deposition sequence) processed with two different ex-situ RTP temperatures of 1000 °C (top 2) and 700 °C (bottom 2), respectively. **c**, Raman spectra of S4 with slower cooling rates.

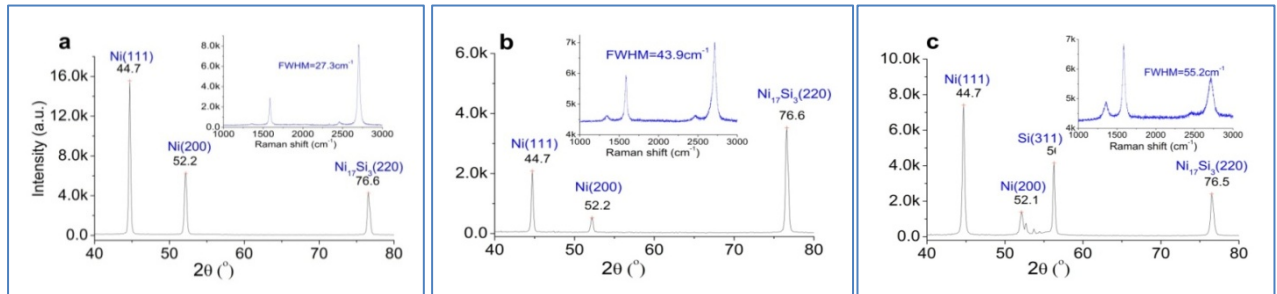


Figure 4| Grazing-incidence diffraction patterns of x-rays for three selected samples.

Panel **a** is for S3 with layers of sub/SiC(50nm)/Ni(500nm), panel **b** for S4 with layers of sub/Ni(500nm)/SiC(50). Both samples were prepared with the same ex-situ RTP condition. Panel **c** is for S2 with layers of sub/SiC(50)/Ni(200nm) which was prepared by in-situ RTP condition. All three samples exhibit preferred Ni(111) and Ni₁₇Si₃(220) crystallographic orientations. The stronger peak intensity of Ni(111) for S3 and Ni₁₇Si₃(220) for S4 suggests that the Ni-silicide concentration across the depth of the films has a gradient distribution, i.e. for S3 the top film surface is Ni rich and for S4 the top surface is Ni-silicide rich. The presence of the Si(311) peak and the weak Ni(200) peak indicates that the re-crystallization and Ni-silicidation process of the sample is incomplete perhaps due to insufficient RTP temperature (650 °C). The in-set in each panel is the corresponding Raman spectrum of the samples for convenience of reference.

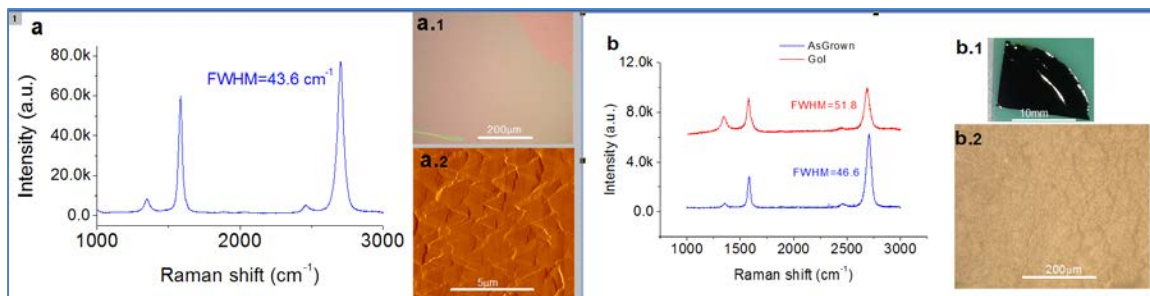


Figure 5| Characterisation of transferred graphene and Gol. **a**, Raman spectrum of graphene settled on Si/SiO₂ substrate after removal of Ni-silicide in HCl. Its optical microscope image is shown in **a.1** and AFM image in **a.2**. The AFM image shows the surface morphology of the graphene is a replica of that of the Ni surface. **b**, Raman spectrum of Gol (red), graphene on the new insulator substrate of SiO₂/Ti/SiO₂, deposited by sputtering after RTP. The Gol is supported on heat-release tape and peeled off from the original substrate. A digital camera picture of the whole peeled-off sample with Ni-silicide/graphene/SiO₂(200nm)/Ti(200nm)/SiO₂(200nm) layer stack on heat release tape is shown in **b.1**. Some wrinkles and damage were evident due to the distortion of the tape caused by the peeling off process. An optical microscope image of the Gol after removal of the Ni-silicide in HCl, is shown in **b.2**. The Raman spectrum in blue is from the as-grown graphene of the same sample scanned before the deposition of the new insulator. As shown by the two spectra, the FWHM value of the 2D band of the Gol increased to 51.8 cm⁻¹ from 46.6 cm⁻¹ of the as-grown graphene. There is also a considerable increase of the D peak intensity, which indicates possible damages of the Gol, which may be caused by the peeling off process, the laser heating effect to the supporting tape during Raman and the sputter-deposition of the new insulator.

Supplementary information

Growth of large area graphene from sputtered films

Genhua Pan¹, Mark Heath¹, David Horsell² and Lesley Wears²*

¹ Wolfson Nanomaterials and Devices Laboratory, Faculty of Science and Technology, University of Plymouth, Devon, PL4 8AA, UK

² College of Engineering, Mathematics and Physical Sciences, University of Exeter, Exeter, EX4 4QF, UK

1. Rapid thermal processing (RTP) and heating/cooling curves

After deposition of the SiC/Ni or Ni/SiC stacks, RTP was carried out either in-situ or ex-situ. Fig.S1 shows the typical heating and cooling curves for the in-situ (red curve) and ex-situ RTP using various conditions (curves of other colours).

Due to the limitations of the equipment of the in-situ RTP as described in Methods, only one RTP condition was used for the work, i.e. heating in vacuum at full power for 10 minutes and switching the power off and cooling down naturally. As can be seen from Fig.S1, it took about 3 minutes for the temperature to reach 600 °C. The temperature rising rate was flattened out for the next 7 minutes with a final temperature of 650 °C. The cooling rate follows an exponential decay curve and it took more than 3 minutes for the temperature to drop down to 300 °C. The temperature was measured by a thermo-couple mounted on the deposition side of the wafer surface.

As described in Methods, the ex-situ RTP apparatus has a much faster heating and cooling rate and also with the choice of two operation modes (intensity or temperature) and RTP parameters. In this work we mainly used the intensity mode. We have found that the best RTP parameters for the samples presented here were ramp-up and ramp-down rate of 15%/s, maximum intensity of 68% and annealing time of 120s, which gives a typical heating cooling curve as shown in Fig.S1 (solid blue curve). As can be seen, for such a condition the temperature of the sample reaches the maximum of 1000 °C almost instantly and the cooling down is also much faster than the in-situ case. Samples were also prepared with other RTP conditions, two typical ones of which were also shown in Fig.S1, where the dotted blue curve was one with the same heating rate, maximum intensity and annealing time, but at a slower ramp-down rate of 1%/s. The major difference is on the cooling rate as in this case the cooling rate was artificially slowed down. The dark-brown curve was for a reduced maximum power intensity of 10% with other parameters kept the same as the solid blue case. As can be seen, the heating-up time increased considerably and the maximum annealing temperature was also reduced to 700 °C. Please refer to Fig.3 for a comparison of Raman spectra of samples prepared under different RTP conditions.

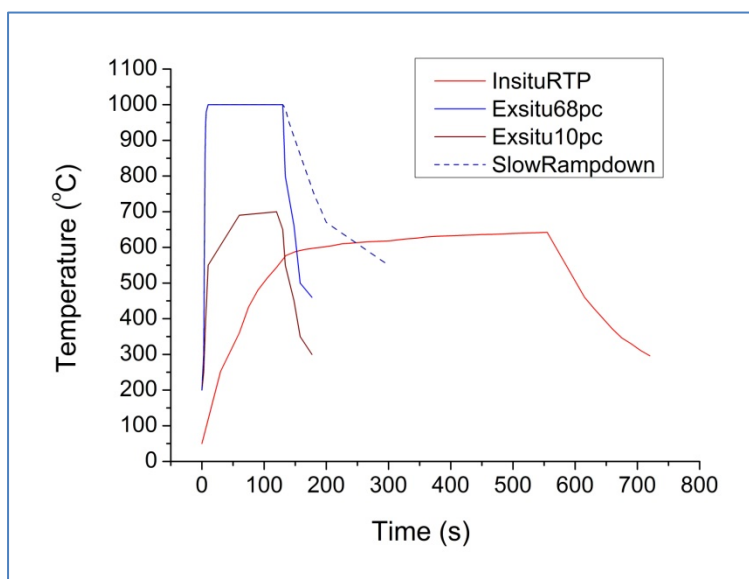


Fig.S1| Typical heating and cooling curves of the in-situ and ex-situ RTP used in the work.

2. Bragg-Brentano geometry and low angle grazing-incidence diffraction patterns of x-rays

X-ray diffraction(XRD) was carried out on selected samples with Bragg-Brentano geometry and grazing-incidence x-ray diffraction at an angle of 1 degree, respectively. The XRD measurements were conducted using a Bruke D8 advanced with a Cu tube. The grazing-incidence diffraction is capable of probing the structure of very thin layers on the sample surface without picking-up the very strong diffraction signal from the Si substrate because the penetration depth of x-rays in grazing-incidence is reduced to 1~10nm from 1~10 μm for the case of Bragg-Brentano geometry. Here we chose the XRD patterns of the two different diffraction modes for a sample with clearly defined shiny (graphene) and dull (non-graphene) areas, as that shown in Fig.2(e), but with layer structure of sub/Ni(500nm)/SiC(50nm) to see whether there is a connection between the graphene formation and crystal phase and orientation. Fig.S2(a) shows the grazing angle diffraction patterns from the shiny area (blue) and dull area (red), respectively. It can be seen although there were considerable differences in the intensities of the diffraction peaks for the two areas, the peak position and relative intensity of the three peaks in each diffraction pattern are very similar, which suggests the crystal phase and their preferred orientations of the two areas are very similar. As has been shown in Fig.2(e), the shiny and dull areas correspond to areas with and without graphene, respectively. The grazing angle XRD patterns of the two areas therefore indicate that there is no connection between the graphene formation and the crystal orientation in these two areas. Fig.S2(b) shows the XRD patterns of the two areas with normal-incidence diffraction, in which the very strong diffraction signals from the Si(400) is dominant due to the deep penetration depth of the x-rays to the sample. On the other hand, the Ni(111) and Ni(200) peaks are hardly visible and the $\text{Ni}_{17}\text{Si}_3(220)$, which is dominant in the grazing-incidence diffraction of Fig.S2(a), became invisible. This again confirms that for samples with SiC on top of the Ni layer, the top surface is Si rich and there is a composition gradient due to the insufficient diffusion cross the depth of the sample.

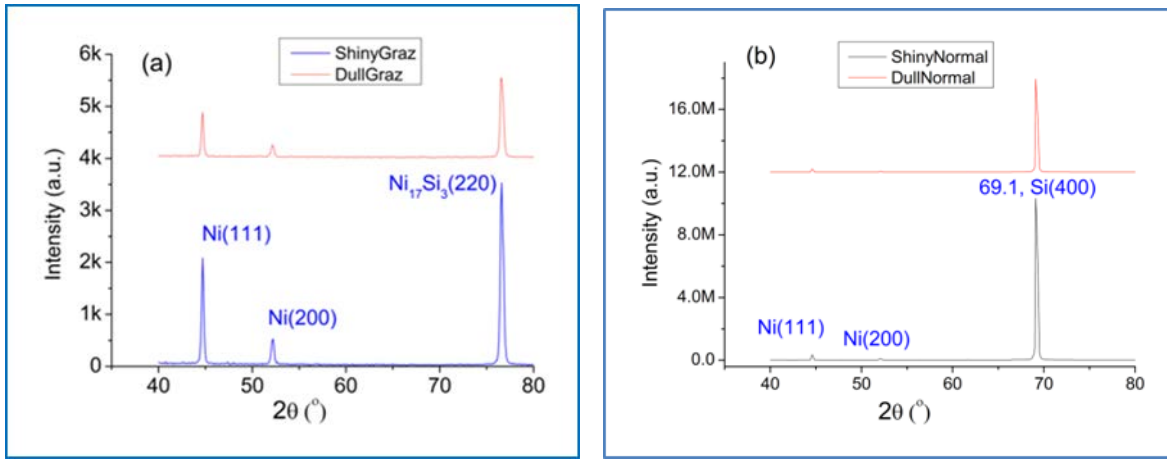


Fig.S2| X-ray diffraction patterns of Bragg-Brentano geometry and low angle grazing-incidence of a sample with layer structure of sub/Ni(500nm)/SiC(50nm) and also with clearly defined shiny and dull areas corresponding to graphene and non-graphene areas, respectively. (a) Grazing angle diffraction patterns from the shiny area (blue) and dull area (red). (b) Bragg-Brentano geometry diffraction patterns for the two areas.

3. Growth of graphene from C/Ni and SiC/Pt films

Graphene can also be produced from C/Ni and SiC/Pt films, which suggests that SiC is merely one of the carbon sources which can be employed for the growth of graphene and other metals may also be used in place of Ni for such a purpose. Here we show in Fig.S3 our initial results by using these two alternative materials. In Fig.S3, the result for the SiC(50nm)/Pt(500nm) (red) was produced by ex-situ RTP and that for C(30nm)/Ni(200nm) was produced by in-situ RTP. No further optimisation has been carried out for the paper for samples with these two materials.

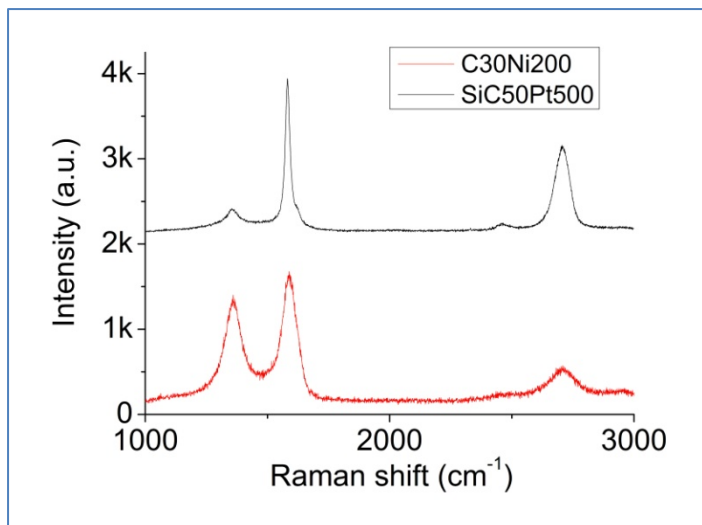


Fig.S3| Raman spectra for samples with layers of C(30nm)/Ni(200nm) (black) and SiC(50nm)/Pt(500nm) (red).

4. Transfer of graphene to a new insulator substrate by vacuum deposition

This was accomplished with the deposition of a tri-layer stack of SiO_2 (200nm)/Ti(200nm)/ SiO_2 (200nm) on to an as-grown graphene sample prepared by ex-situ RTP, the use of heat release tape as additional support to the Gol, peeling-off of the original wafer, etching of the Ni and Ni-silicide layers of the stack, and Raman inspection of the resulting Gol, as shown in Fig.5b. The Ti layer serves as a laser beam blocking layer for the purpose of Raman scan of the Gol. The choice of Ti was because it was perhaps the only material available which doesn't dissolve in HCl and at the same time provides a good adhesion to the SiO_2 layers. Several attempts have been made before that. The initial method used was to deposit a 300 nm-thick SiO_2 layer right after RTP and then remove the metal layer by etching of the sample in HCl for Raman inspection of the Gol. However, the retaining of the Gol after the removal of the metal layer in HCl was unsuccessful due to the very large stress of the SiO_2 layer, which resulted in a complete roll-up of the Gol after the etching of the Ni layer. We have subsequently used a piece of heat release tape as an additional support to the Gol.

Although this could effectively prevent the Gol from rolling-up, it was impossible to obtain any Raman spectrum for the Gol due to the very strong background Raman signal of the tape. We then resorted to the use of a laser-beam blocking layer in a tri-layer configuration as shown above. The first convenient material to try was SiC, however, it dissolved in the HCl solution immediately. Pt layer was second to be used, which didn't dissolve in HCl but its adhesion to the SiO₂ layers was very poor and the tri-layer stack came apart in the wrong place. The Ti was eventually successfully used for such a purpose. The second issue for achieving this vacuum transfer of graphene in the same evacuation as the RTP is the need for a minimum number of 4 sputtering materials (Ni, SiC, SiO₂ and Ti) in the machine equipped with in-situ RTP. This was impossible to achieve for the 3-target machine we have without a vacuum break (change of sputtering target). For this reason, we only demonstrated the Gol process with a sample prepared by ex-situ RTP. Ultimately, the Gol needs to be prepared with in-situ RTP, in-situ deposition of SiO₂, direct Si wafer bonding and the removal of the original Si substrate by Si etcher, as shown in Fig.1(d) and (e), however, this is again constrained by un-availability of these facilities.